Distinct neural networks derived from galanin-containing nociceptors and neurotensin-expressing pruriceptors

Yan Chen[a,c,1], Yuran Song[b,c,1] (ID), Huadong Wang[d,1] (ID), Yiyun Zhang[c,e], Xinyu Hu[c,f], Kaikai Wang[c,e], Yingjin Lu[a], Zoutao Zhang[g], Shuai Li[a,c] (ID), Anan Li[g], Lan Bao[a,e,f], Fuqiang Xu[d], Changlin Li[a,c,h,2], and Xu Zhang[a,c,e,2]

Pain and itch are distinct sensations arousing evasion and compulsive desire for scratching, respectively. It's unclear whether they could invoke different neural networks in the brain. Here, we use the type 1 herpes simplex virus H129 strain to trace the neural networks derived from two types of dorsal root ganglia (DRG) neurons: one kind of polymodal nociceptors containing galanin (*Gal*) and one type of pruriceptors expressing neurotensin (*Nts*). The DRG microinjection and immunosuppression were performed in transgenic mice to achieve a successful tracing from specific types of DRG neurons to the primary sensory cortex. About one-third of nuclei in the brain were labeled. More than half of them were differentially labeled in two networks. For the ascending pathways, the spinothalamic tract was absent in the network derived from *Nts*-expressing pruriceptors, and the two networks shared the spinobulbar projections but occupied different subnuclei. As to the motor systems, more neurons in the primary motor cortex and red nucleus of the somatic motor system participated in the *Gal*-containing nociceptor-derived network, while more neurons in the nucleus of the solitary tract (NST) and the dorsal motor nucleus of vagus nerve (DMX) of the emotional motor system was found in the *Nts*-expressing pruriceptor-derived network. Functional validation of differentially labeled nuclei by c-Fos test and chemogenetic inhibition suggested the red nucleus in facilitating the response to noxious heat and the NST/DMX in regulating the histamine-induced scratching. Thus, we reveal the organization of neural networks in a DRG neuron type-dependent manner for processing pain and itch.

pain | itch | neural network | dorsal root ganglia | herpes simplex virus

Pain and itch are distinct sensations and proposed to be processed in different neural networks. Cutaneous signals of noxious or pruritic stimuli can be detected by free nerve endings of the small-diameter pseudounipolar somatosensory neurons located in the dorsal root ganglion (DRG) (1, 2). Single-cell RNA-sequencing of DRG neurons revealed the DRG neuron populations (3–8). According to single-cell RNA-sequencing data, calcitonin related polypeptide-α (*Calca*), the traditional marker of peptidergic nociceptors (1), was contained in multiple clusters, including two pruritogen-sensitive DRG neuron clusters expressing natriuretic peptide B (*Nppb*) or mas-related grp family member a3 (*Mrgpra3*), respectively (9, 10). Galanin (*Gal*) could be used as a marker to separate the small-dimeter peptidergic neurons from the pruriceptors and c-fiber low-threshold mechanoceptor (3, 6). The population of *Gal*⁺ DRG neurons are composed by several subsets for the detection of noxious mechanoheat and cold (4–6). There are three subsets of pruriceptors, which are marked by *Nppb* (10), *Mrgpra3* (9), and *Mrpgrd* (11), respectively. The *Nppb*⁺ neurons could be also marked by the genes encoding somatostatin (*Sst*) and neurotensin (*Nts*) (3, 6, 7). Both *Gal*⁺ and *Nppb*⁺ DRG neurons project unmyelinated C fibers to the lamina I and outer lamina II in the dorsal horn of spinal cord (12, 13).

In the spinal cord, the nociceptive signals are transmitted to lamina I projection neurons that are gated by interneurons (12). On the other hand, specific spinal circuits for processing itch signals have been identified. For example, the lamina II interneurons expressing NPPB receptor (NPR1) release gastrin-releasing peptide (GRP) and form excitatory synapses with interneurons expressing GPR receptor (GRPR). The GRPR⁺ neurons finally transmit itch signals to lamina I projection neurons in the spinal cord (2). Therefore, there could be different circuits for processing pain and itch in the spinal cord. However, it remains largely unknown whether distinct organizations of supraspinal neural networks exist for perceiving pain and itch.

At the supraspinal level, somatosensory signals are transmitted to the cortex via ascending pathways to encode perception and emotion (14), and simultaneously activate descending pathways to arouse behavioral reaction and descending regulation (15).

Significance

We achieve tracing of neural networks derived from *Gal*-containing or *Nts*-expressing dorsal root ganglia neurons by microinjection of recombinant herpes simplex virus into the lumbar 5 dorsal root ganglia. Immunosuppression effectively facilitated the infection ratio of the viral tracer. By comparing neural networks, we identify differentially labeled nuclei, reveal distinct organization of ascending pathways, and demonstrate different involvement of the somatic motor system and the emotional motor systems in two neural networks. Functional validation of the representative, differentially labeled nuclei suggested the relevance of the neural networks with pain and itch, respectively. This study provides insight into the modality selectivity of supraspinal neural networks for processing pain and itch.

To map the involved nuclei in somatosensory neural networks, an efficient polysynaptic anterograde tracer with low toxicity is required. Currently, the common neurotropic viral tools for anterograde tracing include adeno-associated virus (AAV), herpes simplex virus (HSV), and vesicular stomatitis virus (VSV). VSV is a member of the family *Rhabdoviridae*, genus *Vesiculovirus*, and transmits anterogradely by its G protein (16). However, the high toxicity of VSV leads to a rapid death of animals, resulting a short time window for examination (17). AAV is known for low cellular toxicity but displays limited transsynaptic capability (18). HSV type 1 (HSV-1) has been used as a tracer for the polysynaptic neural circuit for decades (19). The direction of spread is viral strain-dependent. The HSV-1 H129 strain has been identified as an anterograde tracer (20, 21). To restrict the starter neurons in specific cell types, a Cre-dependent antero-grade transsynaptic tracer derived from H129, H129ΔTK-TT, has been developed (22). H129ΔTK-TT HSV Cre-dependently expresses thymidine kinase (TK) and tdTomato. TK is essential for viral replication and tdTomato is expressed for labeling neu-ral networks in which HSV propagates. Nevertheless, this tool has not been reported to trace somatosensory circuits.

In the present study, we injected H129ΔTK-TT HSV directly into the lumbar 5 (L5) DRG and simultaneously treated the mice with immunosuppressant to facilitate the virus infection and propagation, to achieve the labeling of neural net-works derived from the *Gal*$^+$ nociceptors and *Nts*$^+$ pruricep-tors. Comparison of these two neural networks showed that they partially shared the spinobulbar projections but not the spinothalamic tract (STT). Analysis of the differentially labeled nuclei revealed that the *Gal*$^+$ nociceptor-derived network occu-pied the primary motor cortex (MOp) and red nuclei (RN) in the somatic motor system, while the *Nts*$^+$ pruriceptor-derived network contained the nuclei of the solitary tract (NST) and the dorsal motor nucleus of vagus nerve (DMX) in the emo-tional motor system. Moreover, the examination of c-Fos expression and chemogenetic inhibition validated the function of the RN in facilitating the response to noxious heat, and the NST in regulating the histamine-induced scratching behavior. The above evidence demonstrates distinct neural networks at the supraspinal level for pain and itch processing.

Results

Immunosuppression Facilitates HSV Infection in the DRG.

To explore the neural networks from somatosensory neurons to the primary sensory cortex (SSp), we applied HSV as a tracer. This virus naturally prefers somatosensory neurons in primates (23) and is able to propagate anterogradely along the somatosensory circuits. However, it has not been reported to trace somatosen-sory circuits in mice before. Considering that the soma of a somatosensory neuron is assembled in the DRG and its periph-eral terminals are widely distributed in the sensory organs—such as skin, muscle, joint, and viscera—the microinjection was performed to directly deliver the virus into the L5 DRG to achieve the high concentration of virus around the soma. Another troublesome issue for viral tracer is possible immune elimination of the host. Bortezomib, the immunosuppressive agent, is a kind of proteasome inhibitor treating the multiple myeloma (24). It inhibits the proteasome to degrade viral cap-sid (25). Bortezomib has been reported to enhance the infec-tion of AAV in mice (26). Therefore, we tried to apply the DRG microinjection together with bortezomib treatment to facilitate the infection of HSV in the L5 DRG neurons (*SI Appendix*, Fig. S1*A*).

The L5 DRG was exposed by laminectomy. A recombinant H129 strain expressing enhanced green fluorescent protein (EYFP) was delivered into the DRG by a glass electrode. Bortezo-mib (1 mg/kg) was injected intradermally into mice immediately after the viral injection. Six to 7 d later, about 50% neurons, including both small- and large-diameter ones, in the L5 DRG were labeled with EYFP, which was five times more than that in the control group receiving the saline treatment after the viral injection (*SI Appendix*, Fig. S1*B*). In addition, we noticed that the surgery of laminectomy might induce nerve injury caused by improper operations occasionally. Since nerve injury could lead to changes of gene expression in DRG neurons, the mice with significant nerve injury in the DRG were excluded by examining the expression of activating transcription factor 3 (*Atf3*), a gene marker of peripheral nerve injury (*SI Appendix*, Fig. S1*C*). Taken together, the data show that administration of the immunosup-pressive agent immediately after the viral microinjection in the L5 DRG effectively enhances the infection of HSV in mouse DRG neurons.

HSV Efficiently Traces the Somatosensory Neural Networks Derived from *Gal*$^+$ Nociceptors and *Nts*$^+$ Pruriceptors.

To map the neural networks derived from *Gal*$^+$ nociceptors or *Nts*$^+$ pruriceptors, H129ΔTK-TT was injected into the left L5 DRG of the *Gal*-Cre or *Nts*-Cre transgenic mice and allowed to propagate along the somatosensory neural network for 7 d (Fig. 1*A*). The infective ratio of HSV in DRG neurons was examined with tdTomato expression in the *Gal*-Cre and *Nts*-Cre transgenic mice, which were 13.2 ± 0.3% and 11.2 ± 1.0%, respectively (*SI Appendix*, Fig. S2*K*). Average size of labeled neurons in the *Gal*-Cre mice was 478.3 ± 11.8 μm^2 and that in the *Nts*-Cre mice was 517.8 ± 18.9 μm^2, which was in accordance with the size of *Gal*$^+$ and *Nts*$^+$ DRG neu-rons (Fig. 1*B*). In the lumbar DRG, we performed RNAscope in situ hybridization (ISH) combined with immunofluores-cence histochemistry (IHC) to detect the colocalization of *Gal* or *Nts* with tdTomato expressed by H129ΔTK-TT in the injected DRG (*SI Appendix*, Fig. S2 *A* and *C*). In *Gal*-Cre mice, 77.0 ± 3.7% of tdTomato$^+$ DRG neurons expressed *Gal* (*SI Appendix*, Fig. S2*B*), while in *Nts*-Cre mice, 73.1 ± 4.5% of infected neurons expressed *Nts* (*SI Appendix*, Fig. S2*D*). Regarding the difference of efficient of Cre recombinase and the probes used in RNAscope ISH, the percentages of labeling indicated a relatively specific labeling of H129 in the two types of DRG neurons. To further validate the *Gal*-Cre and *Nts*-Cre mouse lines, we injected recombinant AAV, which Cre depen-dently expressed EYFP in the L5 DRG of *Gal*-Cre or *Nts*-Cre mice. Then, we performed RNAscope ISH combined with IHC to examine the colabeling of EYFP with *Gal* or *Nts* in the infected DRG. Results showed that 88.9 ± 2.2% of EYFP$^+$ neurons expressed *Gal* in *Gal*-Cre mice (*SI Appendix*, Fig. S2*B*), and that 86.6 ± 4.2% expressed *Nts* in *Nts*-Cre mice (*SI Appendix*, Fig. S2*D*). These results indicate that the *Gal*-Cre and *Nts*-Cre mouse lines are effective.

The cellular toxicity is a common concern of transsynaptic viral tracers. Release of recombinant HSV from dying neurons would cause nonspecific labeling of starter cells and down-stream neural networks. In order to exclude cases with dying neurons, we examined the expression of Caspase 3, a marker of apoptosis, in the injected DRG, spinal cord, and supraspinal brain regions along the ascending pathways (*SI Appendix*, Fig. S2 *E–J*). Cases with the expression of Caspase 3 were excluded. In addition, we optimized the time-point of killing in order to achieve a balance between the maximal labeling and minimal
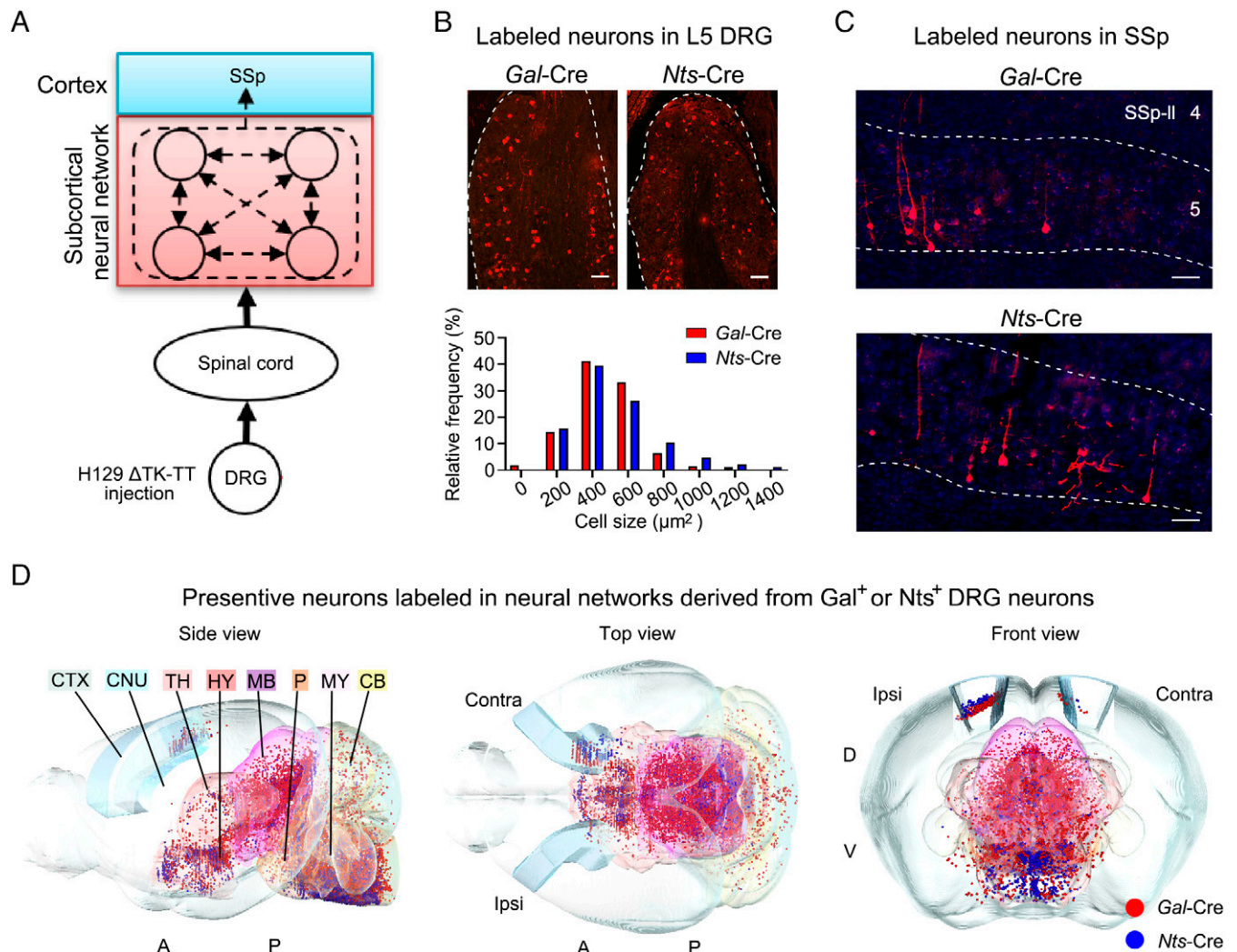
Fig. 1. Tracing neural networks derived from *Gal*+ and *Nts*+ DRG neurons. (*A*) A schematic illustration of viral tracing from DRG to SSp. (*B*, *Upper*) Labeling of small-diameter DRG neurons in transgenic *Gal*-Cre and *Nts*-Cre mice. (Scale bar, 100 μm.) (*Lower*) Histogram showing the distribution of cell size. Average size of labeled neurons in the *Gal*-Cre and *Nts*-Cre mice was in accordance with the size of *Gal*+ and *Nts*+ DRG neurons (for *Gal*-Cre 283 neurons from nine sections/three animals; for *Nts*-Cre 176 neurons from nine sections/three animals). (*C*) Labeling of neurons in SSp demonstrated a successful tracing from the periphery to the cortex. (Scale bar, 100 μm.) (*D*) Representative three-dimensional reconstruction of neural networks derived from the *Gal*+ (red) and *Nts*+ (blue) DRG neurons. One dot represents one labeled neuron. The acronyms in the figures are based on the abbreviations listing in the *SI Appendix*.

toxicity. Thus, we limited the propagation and spread time of HSV within 7 d. According to our observation, it took at least 48 h for HSV to transport from the soma of DRG neurons to the central terminals. Secondary spinal neurons could be labeled at about 72 h after viral injection. Then the virus propagated along the ascending pathways and labeled downstream neural network step by step, as described in Alice McGovern et al.'s report (27). We found that the SSp and MOp were the very first and specific cortical areas that could be labeled (Fig. 1*C*). Therefore, three cases in each group that only the MOp and SSp were labeled in the cortical area were selected for further analysis.

For the analysis of neural networks derived from *Gal*+ and *Nts*+ DRG neurons, labeled neurons in the brain were registered into the three-dimensional Allen Common Coordinate Framework reference atlas (CCFv3) (28) (*SI Appendix*, Fig. S3). The neural networks were reconstructed from the sections of the brain from the Bregma 0.49 mm to −7.83 mm (Fig. 1*D*). Although the infective ratio of DRG neurons was comparable among analyzed mice (*SI Appendix*, Fig. S2*K*), the total number of labeled neurons in the brain ranged from 5,000 to 20,000 in both

networks. To exclude the interference of differential infection efficiency, we normalized the number of labeled neurons in each nucleus to that in the whole brain, namely the labeling percentage to represent the organization of networks.

Since the propagation speed of HSV in mice was inconsistent, the difference of labeled networks may be caused by the delayed or speeded propagation. Given that the SSp is known as the cortical target of the ascending pathway, three mice with similar labeled percentage (0.2 ± 0.1%) at the SSp were selected from each group in order to compare the networks derived from *Gal*+ and *Nts*+ DRG neurons (*SI Appendix*, Fig. S2*L*). To further ensure that the networks derived from a same type of DRG neurons are repeatable, we detected the correlation coefficient of the signal distribution among the networks of selected mice in one group. As expected, the labeling pattern of neural networks derived from the same type of DRG neurons was consistent among mice (*SI Appendix*, Fig. S2*M*). Thus, the somatosensory neural networks derived from *Gal*+ and *Nts*+ DRG neurons are efficiently traced and quantified, which provides a basis for further comparison of these two networks.
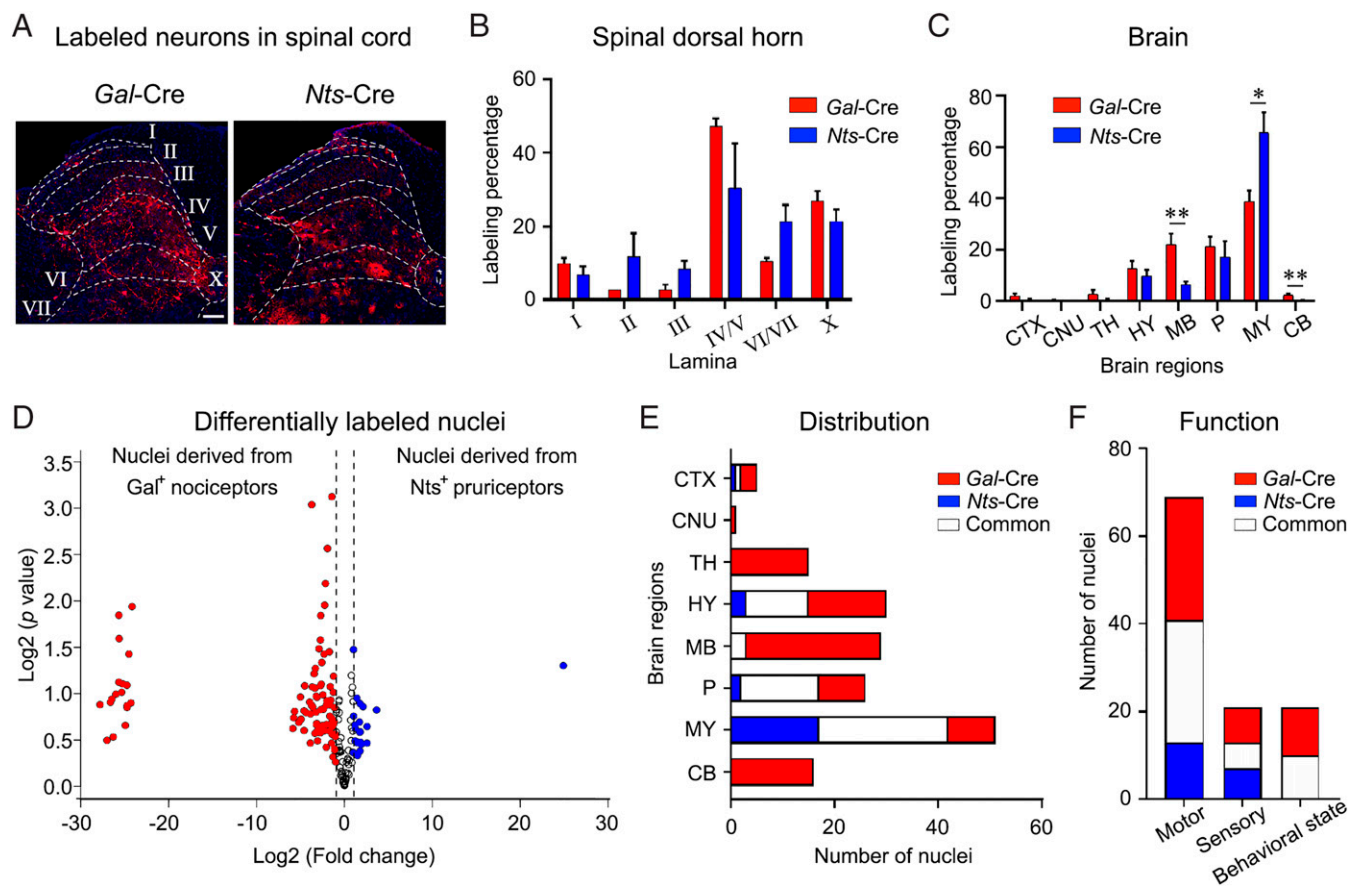
Neural Networks Derived from *Gal*⁺ Nociceptors and *Nts*⁺ Pruriceptors Are Differentially Organized at the Supraspinal Level. Neural networks derived from DRG neurons can be roughly divided into spinal and supraspinal neural networks. To explore the anatomic difference in the spinal neural networks derived from *Gal*⁺ and *Nts*⁺ DRG neurons, we counted the number of labeled neurons in each lamina of the spinal cord and compared the distribution of labeled neurons (Fig. 2 *A* and *B*). In both spinal neural networks, labeled neurons were observed in the lamina I–X of the spinal dorsal horn. In lamina I, the percentage of labeled neurons was 9.86 ± 1.41% and 6.80 ± 3.24% in the spinal neural networks derived from *Gal*⁺ and *Nts*⁺ DRG neurons, respectively. A tendency appeared that more interneurons in lamina II and III were labeled in the spinal neural network derived from *Nts*⁺ DRG neurons. In lamina II, the percentage of labeled neurons derived from *Gal*⁺ nociceptors was 2.8 ± 0.0% in the spinal dorsal horn, and that derived from the *Nts*⁺ pruriceptors was 11.7 ± 6.5%. In lamina III of the spinal dorsal horn, the percentages were 2.8 ± 1.4% and 8.5 ± 2.1% in labeling neurons derived from the *Gal*⁺ nociceptors and *Nts*⁺ pruriceptors, respectively. More than half

of labeled neurons were in the deep laminae (lamina IV and V) in both spinal neural networks. Thus, the distribution of labeled neurons in the spinal neural networks derived from *Gal*⁺ and *Nts*⁺ DRG neurons displays similar pattern.

In the supraspinal neural networks derived from both types of DRG neurons, most labeled neurons were detected in the subcortical areas including interbrain, midbrain, and hindbrain. Importantly, the distribution patterns of labeled nuclei derived from two types of DRG neurons exhibited largely different in the subcortical area (Fig. 2*C*). The labeling percentage in the midbrain derived from *Gal*⁺ DRG neurons was 21.9 ± 2.5%, much higher than that derived from *Nts*⁺ DRG neurons (6.5 ± 0.7%). In contrast, the labeling percentage in the medulla derived from *Nts*⁺ DRG neurons (65.6 ± 4.5%) was much higher than that derived from *Gal*⁺ DRG neurons (38.7 ± 2.5%). Besides the subcortical area, the difference was also observed in the cerebellum derived from two types of DRG neurons. The labeling percentage in the cerebellum derived from *Gal*⁺ DRG neurons (2.2 ± 0.3%) was higher than that derived from *Nts*⁺ DRG neurons (0.3 ± 0.1%). These data suggest that *Gal*⁺ nociceptors and *Nts*⁺ pruriceptors present distinct neural networks, especially at the supraspinal level.

Fig. 2. Quantitative analysis of neural networks derived from *Gal*⁺ and *Nts*⁺ DRG neurons. (*A*) A transverse section of the lumbar spinal cord showing the distribution of labeled neurons on the ipsilateral spinal dorsal horn. (Scale bar, 100 μm.) (*B*) Quantification of labeled neurons in each lamina of the lumbar spinal cord. Data are shown as mean ± SEM (comparisons by two-tailed unpaired *t* test: n.s., *P* > 0.05, *n* = 3 for each group). The distribution of labeled neurons in the spinal neural networks derived from *Gal*⁺ and *Nts*⁺ DRG neurons displayed similar pattern with slight difference in the lamina II–III. (*C*) Quantification of labeled neurons in major regions of the brain. Data are shown as mean ± SEM. The labeling percentage of brain regions were compared between two networks (comparisons by two-tailed unpaired *t* test: **P* < 0.05, ***P* < 0.005, *n* = 3 for each group). The labeling percentages in the midbrain and cerebellum were higher in the *Gal*–Cre mice, while the labeling percentage in the medulla was higher in *Nts*-Cre mice. (*D*) Volcano plot showing the differentially labeled nuclei in two neural networks defined as those showing more than two times of differences. The log₂ (fold-change) indicates the mean labeling percentage for each nucleus (*n* = 3 for each group). Each dot represents one nucleus. Red dots represent differentially labeled nuclei derived from the *Gal*⁺ DRG neurons; blue dots represent differentially labeled nuclei derived from the *Nts*⁺ DRG neurons; hollow dots represent common nuclei. (*E*) Histogram showing the distribution of differentially labeled nuclei and common nuclei in major regions of the brain. The medulla involved more in the *Nts*⁺ pruriceptor-derived network, while the *Gal*⁺ nociceptor-derived network was widely dispersed in the brain. (*F*) Histogram showing the distribution of differentially labeled nuclei and common nuclei with functions related to motor, sensation, or behavioral states. Most of the differentially labeled nuclei were related to motor function.

We further counted nuclei labeled constantly among mice in the supraspinal neural networks from each group. Labeled neurons were detected in 405 annotated nuclei, including 175 nuclei in the Gal^+ nociceptor-derived network (*SI Appendix,* Table S1) and 118 nuclei in the Nts^+ pruriceptor-derived network (*SI Appendix,* Table S2). There were 96 common nuclei in two neural networks thatp were defined as those presenting fewer than two times of difference, including the contralateral SSp-ll in the cortex, the paraventricular hypothalamic nucleus in the hypothalamus, the ventral tegmental area in the midbrain, the parabrachial nucleus (PB) in the pons, and the nucleus raphe in the medulla (*SI Appendix,* Table S3). The differentially labeled nuclei in two neural networks were defined as those showing more than two times of the differences (Fig. 2D), including the MOp in the cortex, the ventral posterolateral nucleus of the thalamus (VPL), the dorsomedial nucleus of the hypothalamus, the RN in the midbrain, the pontine reticular nucleus in the pons, as well as the NST, and DMX in the medulla, and so forth (*SI Appendix,* Table S3).

The differentially labeled nuclei from the Nts^+ pruriceptor-derived network were mainly located in the medulla, while those from the Gal^+ nociceptor-derived network were widely dispersed in the brain (Fig. 2E). According to the annotation of the Allen Adult Mouse Atlases (atlas.brain-map.org/), which follows the global modal of cerebral hemisphere organization proposed by Larry W. Swanson (29), we further classified the common nuclei and differentially labeled nuclei in the cortex, midbrain, and hindbrain as motor, sensory, and behavioral state-related nuclei (Fig. 2F). The behavioral state-related nuclei refer to those regulating the sleep–wake cycle and arousal level during waking. Among them, 69, 21, and 21 nuclei were related to the function of motor, sensory, and behavioral state, respectively. In the 69 motor-related nuclei, 28 of them were differentially labeled nuclei in the nociceptor-derived network (*SI Appendix,* Table S4). Taken together, these data show that the supraspinal neural networks derived from Gal^+ nociceptor and Nts^+ pruriceptor present distinct organization of nuclei, suggesting differential neural mechanisms in processing pain and itch.

Ascending STT and Spinobulbar Projection Are Differentially Involved in Neural Networks Derived from *Gal*$^+$ Nociceptors and *Nts*$^+$ Pruriceptors. The somatosensory ascending pathway includes the projections from the spinal cord to the contralateral VPL via the STT and to the homeostatic control regions via the spinobulbar projection, including the rostral ventromedial medullar (RVM), the PB in the pons, and the periaqueductal gray (PAG) in the midbrain (*SI Appendix,* Fig. S4 *A* and *B*). For the STT, 0.14 ± 0.10% of signals were observed in the contralateral VPL in the Gal^+ nociceptor-derived network. Although participation of the STT in processing itch has been reported in primates (30), signals in the VPL were not observed in the Nts^+ pruriceptor-derived network in mice (Fig. 3A and *SI Appendix,* Fig. S4C). This evidence makes us to query the role of VPL in processing itch in rodents. One possibility is that $Mrgpra3^+$ or $Mrgprd^+$ pruriceptors sending projections to the VPL for the discriminative component of itch.

For the spinobulbar projection, labeling percentages of the PB (Fig. 3B) and RVM (Fig. 3C) were similar between two networks. In the Gal^+ nociceptor-derived network, 0.8 ± 0.1% of labeled neurons were in the PB, and 9.2 ± 1.8% were located in the RVM including the reticular formation and the nucleus raphe. In the Nts^+ pruriceptor-derived network, 1.0 ± 0.3% and 9.1 ± 0.4% of labeled neurons were in the PB and RVM,

respectively. The major difference of the spinobulbar projection between two networks was present in the PAG (Fig. 3D). The labeling percentage of the PAG in the Gal^+ nociceptor-derived network (9.9 ± 1.1%) was higher than that in the Nts^+ pruriceptor-derived network (3.9 ± 0.6%). Furthermore, the distribution of labeled neurons in the PAG was different between two neural networks (Fig. 3E). We compared the percentage of labeled neurons from subnuclei in the PAG between two networks. In the Gal^+ nociceptor-derived network, labeled neurons were dispersed in the dorsomedial PAG (DMPAG), lateral PAG (LPAG), and ventrolateral PAG (VLPAG), while in the Nts^+ pruriceptor-derived network, labeled neurons were concentrated within the VLPAG. Significantly, the percentage of labeled neurons in the LPAG derived from Gal^+ nociceptors (31.7 ± 3.2%) were nearly three times higher than that derived from Nts^+ pruriceptors (13.9 ± 3.3%) (Fig. 3F). In contrast, the labeled neurons in the VLPAG derived from Nts^+ pruriceptors (38.4 ± 12.2%) tended to be higher than that derived from Gal^+ pruriceptors (25.1 ± 2.7%) (Fig. 3G). These results suggest that the ascending pathways derived from Gal^+ nociceptors and Nts^+ pruriceptors involve different subnuclei of PAG in the spinobulbar projection. Taken together, the data show that the STT is bypassed in the neural network derived from Nts^+ pruriceptors, while two networks share the spinobulbar projections but occupy different subnuclei (Fig. 3H).

To validate the specificity of the subnuclei of PAG in response to noxious or pruritic stimuli, we detected the c-Fos expression in neurons of the LPAG and VLPAG after a hotplate stimulation at 45 °C or an intraplantar injection of 10 μL histamine at the concentration of 25 g/mL (Fig. 3I). Since the viral tracing was started from the lumbar DRG and downstream neural networks were presumably connected to the starter DRG neurons synaptically, we applied either noxious or pruritic stimuli on hind paws of mice, which was innervated by lumbar DRGs and expected activation of neural networks related to these stimuli. Although not all neurons in the brain express c-Fos when they are activated, both noxious and pruritic stimuli can induce c-Fos expression in the PAG (31, 32). In the LPAG, the 45 °C thermal stimuli increased the number of c-Fos$^+$ neurons more than 20 times, while histamine did not induce the c-Fos expression in neurons of this subnucleus (Fig. 3J), in accordance with the relatively more labeling of the LPAG derived from Gal^+ nociceptors than Nts^+ pruriceptors. In the VLPAG, both noxious heat and histamine injection induced c-Fos expression (Fig. 3K), in accordance with the similar labeling percentage of the VLPAG traced from both Gal^+ nociceptors and Nts^+ pruriceptors. Noxious heat induced 10 times of c-Fos expression compared with stimulation of room temperature in the VLPAG. Histamine injection induced about two times of c-Fos expression compared with saline injection. This evidence suggests that the activity of neurons in subnuclei of the PAG could be consistent with the HSV labeling of neurons.

Somatic and Emotional Motor Systems Differentially Participate in Neural Networks Derived from *Gal*$^+$ Nociceptors and *Nts*$^+$ Pruriceptors. The somatosensory neural network includes not only an ascending pathway but also motor systems (33). Noxious stimulation usually leads to the evasive action, and itch often results in a restless and compulsive desire of scratching (34). As mentioned above, more than half of the differentially labeled nuclei were related to motor functions. Next, we analyzed the involvement of the motor system in two neural networks (*SI Appendix,* Fig. S5A). The motor system is divided into the
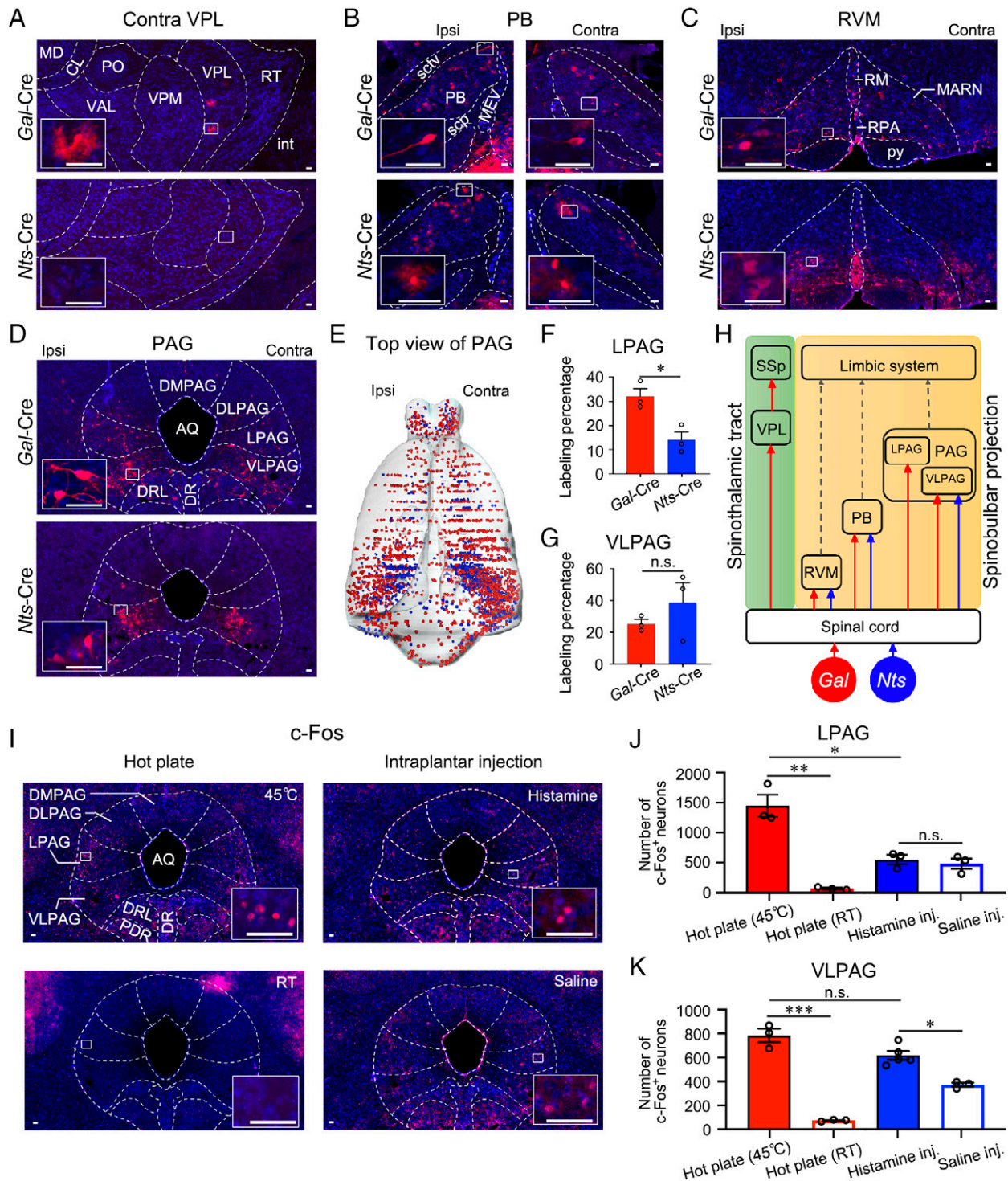
Fig. 3. Differential involvement of ascending pathways derived from *Gal*+ and *Nts*+ DRG neurons. (*A*) Distribution of neurons in the VPL on the contralateral (Contra) side of *Gal*-Cre and *Nts*-Cre mice. (Scale bars, 50 μm.) Signals in the VPL were absent in the *Nts*+ pruriceptor-derived network in mice. (*B* and *C*) Distribution of neurons in the PB on ipsilateral (Ipsi) and contralateral sides, as well as in the RVM. (Scale bars, 50 μm.) No significant difference was found in the PB and RVM. (*D*) Distribution of neurons in different subnuclei of PAG. (Scale bars, 50 μm.) (*E*) Representative top view of the three-dimensional illustration showing the distribution of labeled neurons in different subnuclei of PAG derived from the *Gal*+ (red) or *Nts*+ (blue) DRG neurons. One dot represents one labeled neuron. (*F* and *G*) Quantification of labeled neurons in LPAG and VLPAG derived from the *Gal*+ and *Nts*+ DRG neurons. Data are shown as mean ± SEM (comparisons by two-tailed unpaired *t* test: *P < 0.05; n.s., P > 0.05; n = 3 for each group). *D-G* show that different subnuclei of PAG were occupied in neural networks derived from *Gal*+ and *Nts*+ DRG neurons. (*H*) Schematic summary of the anatomic distinction between ascending pathways derived from the *Gal*+ and *Nts*+ DRG neurons. (*I*) Distribution of c-Fos+ neurons in PAG induced by different stimuli including the hot-plate at 45 °C or room temperature (RT), and the intraplantar injection of 10 μL histamine at the concentration of 25 g/mL or the same volume of saline. (Scale bars, 50 μm.) (*J*) Quantification of c-Fos+ neurons in LPAG induced by the different stimuli. Data are shown as mean ± SEM (comparisons by two-tailed unpaired *t* test: *P < 0.05; **P < 0.005; n.s., P > 0.05, n = 3 for each group). (*K*) Quantification of c-Fos+ neurons in VLPAG induced by the different stimuli. Data are shown as mean ± SEM (comparisons by two-tailed unpaired *t* test: *P < 0.05; **P < 0.005; ***P < 0.0001; n.s. P > 0.05, n = 3 for hot-plate, RT, and saline group, n = 5 for histamine group). The activity of neurons in subnuclei of the PAG was in accordance with the labeling of HSV.
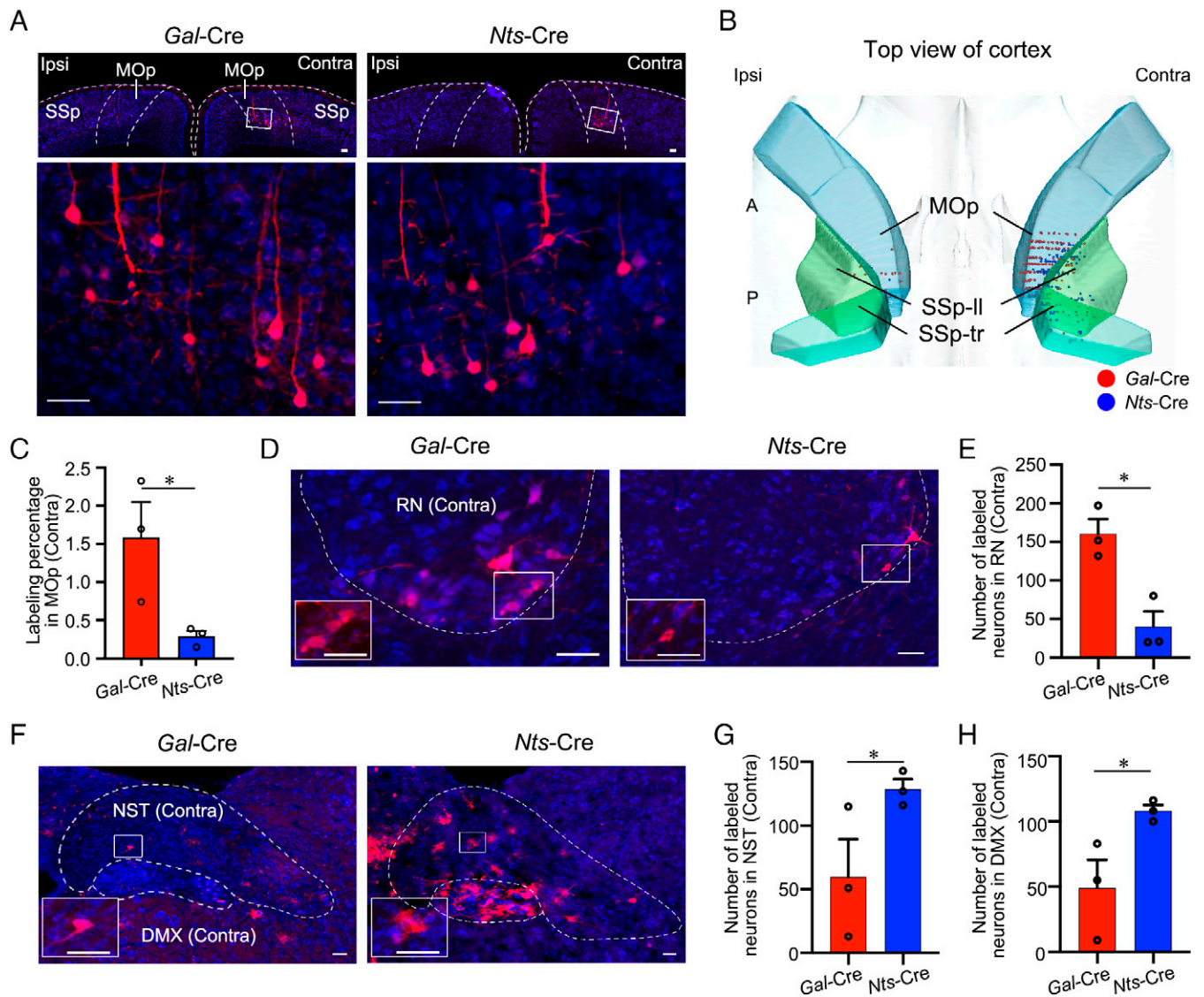
Fig. 4. Differential labeling of nuclei in motor systems derived from *Gal*⁺ and *Nts*⁺ DRG neurons. (*A*) Distribution of neurons in the MOp derived from the *Gal*⁺ and *Nts*⁺ DRG neurons. (Scale bars, 50 μm.) (*B*) Representative top view of the three-dimensional illustration showing the distribution of labeled neurons in the cortical areas derived from the *Gal*⁺ (red) or *Nts*⁺ (blue) DRG neurons. One dot represents one labeled neuron. (*C*) Quantification of labeled neurons in contralateral MOp derived from the *Gal*⁺ and *Nts*⁺ DRG neurons. Data are shown as mean ± SEM (comparisons by two-tailed unpaired t test: *$P <$ 0.05, $n = 3$ for each group). *A*–*C* show that MOp was involved more in the *Gal*⁺ nociceptor-derived network rather than the *Nts*⁺ pruriceptor-derived network. (*D* and *E*) Distribution (*D*) (Scale bars, 50 μm) and quantification (*E*) of labeled neurons in the contralateral RN derived from the *Gal*⁺ and *Nts*⁺ DRG neurons. Data are shown as mean ± SEM (comparisons by two-tailed unpaired t test: *$P <$ 0.05, $n = 3$ for each group). RN was involved more in the *Gal*⁺ nociceptor-derived network. (*F*–*H*) Distribution (*F*) (Scale bars, 50 μm) and quantification (*G* and *H*) of labeled neurons in contralateral NST and DMX derived from the *Gal*⁺ and *Nts*⁺ DRG neurons. Data are shown as mean ± SEM (comparisons by two-tailed unpaired t test: *$P <$ 0.05, $n = 3$ for each group). NST and DMX were involved more in the *Nts*⁺ pruriceptor-derived network.

somatic motor system and emotional motor system (1). The somatic motor system consists of the medial part, including the dorsal part of pontine and medullary medial tegmentum, and the lateral part contains the RN and MOp. In the *Gal*⁺ nociceptor-derived network, labeled neurons were on both sides of the MOp. However, in the *Nts*⁺ pruriceptor-derived network, the signals were absent on the ipsilateral side of the MOp (Fig. 4 *A* and *B*). On the contralateral side, labeled neurons in the MOp derived from *Gal*⁺ nociceptors (1.6 ± 0.5%) were five times more than that derived from *Nts*⁺ pruriceptors (0.3 ± 0.1%) (Fig. 4*C*). A previous study reported that the contralateral descending pathway of the MOp controlled the independent movement of extremities in concert with the RN (35). We found that the number of labeled neurons in the ventral lateral part of the contralateral RN derived from *Gal*⁺ nociceptors (160.3 ± 19.2) was higher than that derived from

Nts⁺ pruriceptors (40.3 ± 19.8) (Fig. 4 *D* and *E* and *SI Appendix*, Fig. S5*B*). Thus, the somatic motor system tends to be involved more in the neural network derived from *Gal*⁺ nociceptors.

On the other hand, the emotional motor system is closely connected with the limbic system (36). The PAG also plays a central role in the emotional motor system. LPAG receiving inputs from the dorsomedial hypothalamus (37) and limbic systems (38) was involved in the network derived from *Gal*⁺ nociceptors as mentioned above. In contrast, the number of labeled neurons in the NST and the DMX derived from *Nts*⁺ pruriceptors (536.3 ± 24.9) were two times more than that derived from *Gal*⁺ nociceptors (245.3 ± 108.4) (Fig. 4*F*), and the number of labeled neurons in contralateral NST (128.7 ± 7.8) and DMX (108.0 ± 4.6) in the neural network derived from *Nts*⁺ pruriceptors was more constant among the examined mice

than that derived from Gal^+ nociceptors (NST: 59.7 ± 29.8; DMX: 49.0 ± 21.57) (Fig. 4 *G* and *H* and *SI Appendix*, Fig. S5*B*). The NST and DMX are known to receive projections from the infralimbic cortex, which is considered as the visceral motor cortex (39). Their roles in modulation of itch sensation have not been studied. Therefore, in the emotional motor system, the neural network derived from Gal^+ nociceptors contains LPAG, while more neurons in the NST and DMX are involved in the neural network derived from Nts^+ pruriceptors.

RN Modulates Pain while NST/DMX Regulates Itch. To validate the functional specificity of RN and NST/DMX, we examined the expression of c-Fos in the RN and NST/DMX in response to noxious or pruritic stimuli applied on hind paws of mice. The c-Fos expression in neurons at the ventral lateral part of the RN could be activated by the hot-plate stimulation at 45 °C (Fig. 5*A*) but not by the intraplantar injection of 10 μL histamine at the concentration of 25 g/mL at the left hind paw (Fig. 5*B*). In neurons of the NST/DMX, 45 °C stimuli induced a sparse expression of c-Fos (Fig. 5*D*), but the histamine injection could induce a dense expression of c-Fos (Fig. 5*E*). Since the caudal part of NST also receives ascending nociceptive information, we noticed that injection of saline on the hind paw also induced c-Fos expression in the NST. To further validate the involvement of the NST in itch-related neural networks, we examined the expression of c-Fos induced by intradermal injection of histamine into the back neck, which represented an established itch behavioral test. We observed c-Fos expression in the NST/DMX but not in the RN (Fig. 5 *C* and *F*). To sum up, neurons in the RN could be activated by the hot-plate but not by the histamine injection (Fig. 5*G*); neurons in the NST/DMX could be activated both by intraplantar and intradermal injection of histamine (Fig. 5 *H* and *I*). Intraplantar injection of saline induced c-Fos expression in the NST/DMX which may be caused by pain. However, intradermal injection of saline in the back neck didn't induce any c-Fos expression in the NST/DMX (Fig. 5 *H* and *I*). The correlation between the nuclei expressing c-Fos induced by distinct modalities of stimuli and the HSV labeling derived from specific type of DRG neurons suggests the functional specificity of the RN in pain, and NST and DMX in itch.

To further validate the functions of differentially labeled nuclei between these two networks, we investigated the roles of the RN and NST/DMX in the modulation of pain and itch. The recombinant AAV with a general *Ef1α* promoter driving the expression of hM4Di was delivered into the locus of the RN or NST/DMX by stereotaxic microinjection (Fig. 5*J*). The hM4Di is a modified form of the human M4 muscarinic (hM4) receptor. It can be activated by the inert clozapine metabolite clozapine-*N*-oxide (CNO) and to silence the activity of all infected cells in the injected nuclei via the Gi signaling pathway (40). In the hot-plate test, the noxious heat stimulus at 52 °C was sufficient to induce c-Fos expression in the RN and to arouse evasive actions. The duration of mice in response to 52 °C was prolonged when the activity of the RN, but not the NST/DMX, was blocked after CNO treatment (Fig. 5*K*). Silencing of the RN also increased the latency of hind paw withdraw in response to noxious radiant heat (*SI Appendix*, Fig. S6*A*). We performed an open-field test and rotarod tests to exclude the impairment of locomotor ability when the activity of cells in RN was blocked. We found that silencing of RN increased the exploratory locomotor activity of mice (*SI Appendix*, Fig. S6*B*), but put no impact on locomotor coordination and balance of mice (*SI Appendix*, Fig. S6*C*). These

results indicated that the delayed response of mice might not be caused by impairment of locomotor ability. On the other hand, since the genes encoding receptors for histamine (*Hrh1*) and serotonin (*Htr2a*) are expressed in the Nts^+ pruriceptors (3), we tested the scratching behavior induced by intradermal injection of histamine (Fig. 5*L*) or 5-HT (*SI Appendix*, Fig. S6*D*) at the back neck. The number of scratches was reduced in both tests when the activity of NST/DMX was inhibited after CNO treatment. Such an effect was not present when the RN was silenced (Fig. 5*L*). Participation of NST/DMX in regulation of itch-induced scratching behavior may imply a role of physiological activities in itch. However, the silencing of the whole complex of NST/DMX had no impact on the blood pressure and heart rate of mice under the resting state (*SI Appendix*, Fig. S6 *E* and *F*), implying the complexity of neural circuits arising from the NST/DMX in modulation of cardiovascular activities. These results suggest the functional significance of the RN and NST/DMX selectively in processing pain and itch, respectively.

Discussion

Recent progresses in cataloging somatosensory neurons with single-cell RNA-sequencing and tracing neural networks with viral tools provide opportunity to explore the neural networks of somatosensory transmission. The present study improved viral strategies to successfully map somatosensory neural networks derived from Gal^+ nociceptors and Nts^+ pruriceptors. Anatomic distinction of these two networks including differentially labeled nuclei provides the specific supraspinal pathways for the processing of heat-evoked withdrawal responses and pruritogen-evoked scratching. For the ascending processing, the neural networks derived from Gal^+ nociceptors and Nts^+ pruriceptors share the spinobulbar projection but not the STT. In the motor system, the Gal^+ nociceptor-derived network tends to be more involved in the somatic motor system, while the Nts^+ pruriceptor-derived network tends to participate in the emotional reaction (*SI Appendix*, Fig. S7). Accordingly, noxious stimuli activate RN in the lateral somatic motor system, which may arouse evasive actions, while pruritic stimuli trigger NST/DMX in the emotional motor system, which may underlie the production of a compulsive desire for scratching. This study not only reveals the morphological organization of neural networks derived from specific types of nociceptors and pruriceptors, but also suggests the functional selectivity of supraspinal neural networks for processing different defense reactions caused by noxious heat or histamine stimulation.

Polysynaptic Tracing of Somatosensory Neural Networks Using HSV. The HSV, as a neurotrophic virus, has been used as an anterograde polysynaptic neural circuit tracer for decades (19). First, it has a wide range of hosts, including the rodent (41), and the amplification and propagation efficiency of HSV is high in mice. Second, the genome size of HSV is more than 150 kb, which is much bigger than that of AAV and provides great loading capacity to carried exogenous genes (19). Third, as a DNA virus it is compatible with the site-specific recombinase system, which makes the Cre- or Flp-dependent recombination of viral genome easy to achieve. Therefore, HSV is an optimal tracer to trace the somatosensory neural network.

The limitations using HSV as a tracer include its toxicity and the individual difference of infective efficiency. To some extent, the toxicity is a common problem for all viral tracers. The strong toxicity of virus hardly allows the postinfection
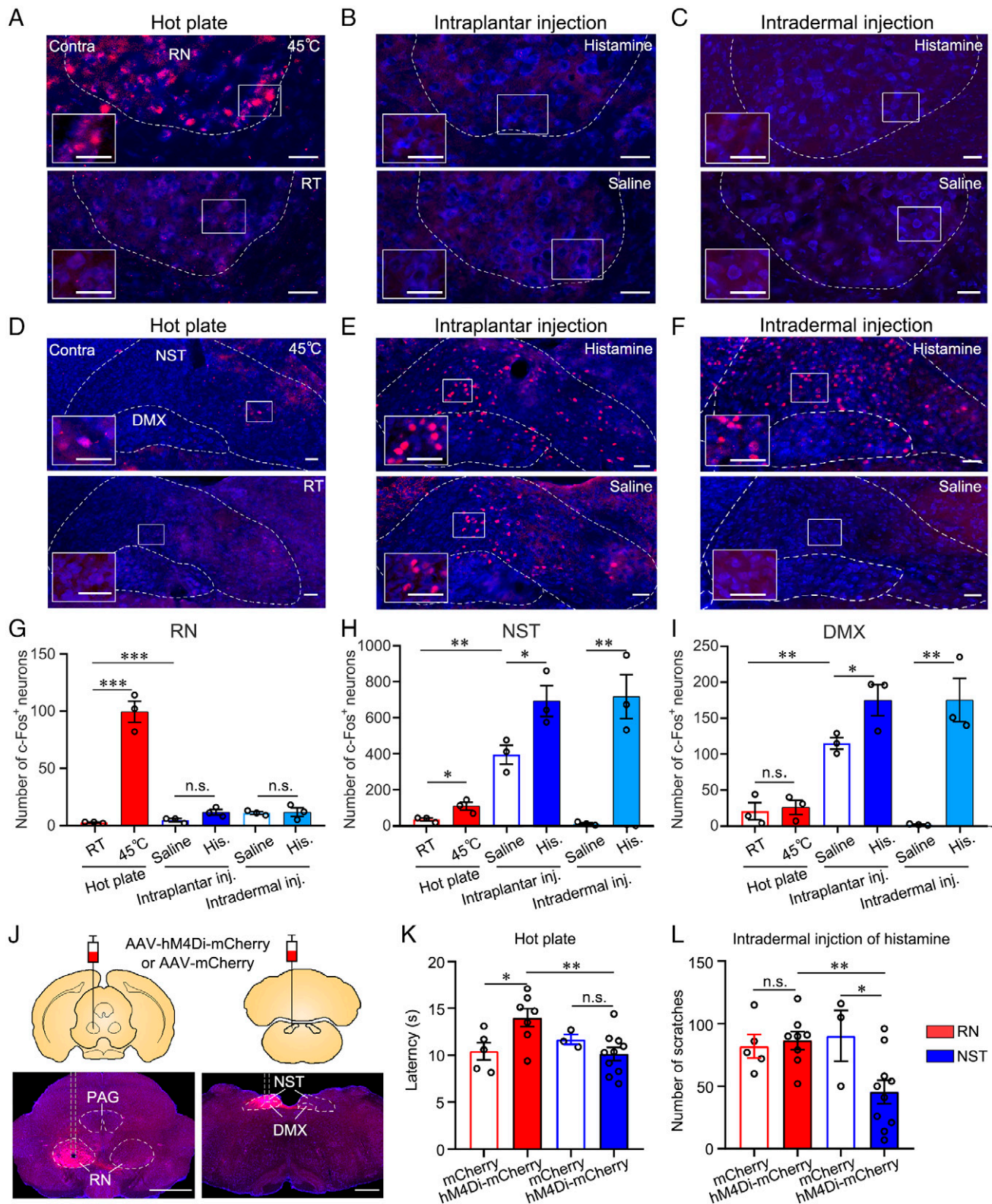
Fig. 5. Functional specificity of RN and NST/DMX in modulation of pain and itch. (*A–C*) Distribution of c-Fos$^+$ neurons in the contralateral (Contra) RN induced by different stimuli, including the hot-plate at 45 °C or room temperature (RT), the intraplantar injection of histamine, or saline at a hind paw, and the intradermal injection of histamine or saline at the back neck. (Scale bars, 50 μm.) (*D–F*) Distribution of c-Fos$^+$ neurons in the contralateral (Contra) NST/DMX induced by different stimuli as described above. (Scale bars, 50 μm.) (*G–I*) Quantification of c-Fos$^+$ neurons in the contralateral RN, NST, and DMX induced by the different stimuli. Data are shown as mean ± SEM (comparisons by two-tailed unpaired *t* test: *$P < 0.05$; **$P < 0.005$; ***$P < 0.0001$; n.s. $P > 0.05$, $n = 3$ in each group). *A–C* and *G* show that noxious heat but not histamine-induced c-Fos expression in RN. *D–F*, *H*, and *I* show that histamine but not noxious heat induced c-Fos expression in NST and DMX. (*J, Upper*) Schematic illustration of stereotaxic injection in RN or NST/DMX. (*Lower*) Distribution of infected cells in RN or NST/DMX. (Scale bars for RN, 1 mm; scale bars for NST/DMX, 500 μm) (*K*) Quantification of the latency in mice responding to hot-plate. Data are shown as mean ± SEM (comparisons by two-tailed unpaired *t* test: *$P < 0.05$; **$P < 0.005$; n.s., $P > 0.05$, $n = 5, 8, 3, 10$ for RN mCherry, RN hM4Di, NST mCherry, and NST hM4Di). (*L*) Quantification of the scratching number in mice responding to subcutaneous injection of histamine. Data are shown as mean ± SEM (comparisons by two-tailed unpaired *t* test: *$P < 0.05$; **$P < 0.005$; n.s., $P > 0.05$, $n = 5, 8, 3, 10$ for RN mCherry, RN hM4Di, NST mCherry, and NST hM4Di). *J–L* show that RN and NST/DMX participated in processing pain and itch, respectively.

time required to trace the whole neural network. As to the H129 ΔTK-TT, the animals with viral injection at the L5 DRG could survive for more than 6 d, which is acceptable for the present study. Differential immunity of mice leads to the individual difference of infective efficiency. With the help of the immunosuppressive agent bortezomib, we achieved a high infective ratio of HSV. Whether other immunosuppressive agents may increase the infection of HSV in DRG neurons needs to be further explored.

Since the feature of polysynaptic infection of HSV, it is difficult to determine the order of a nucleus labeled by HSV in the neural network. The variation in labeling pattern could be caused by different propagation stages of HSV. In the present study, we only analyzed cases at least labeled by HSV in the primary sensory and motor cortex, the fourth order of the somatosensory neural network. Although the total number of labeled neurons varied among the mice, the distribution pattern was similar in the neural network derived from the same type of DRG neurons, suggesting that the subcortical neural network is labeled at a similar level. Further elucidation of the order in the neural network requires the help of other neurotropic viruses, such as AAV and rabies virus.

Anatomic Distinction of Neural Networks for Pain and Itch. Pain and itch are distinct sensations arousing different defense reactions and may be processed in different neural networks. This hypothesis has been proved in the neural network of spinal cord (13, 42, 43). However, due to the lack of gene markers to discriminate the projection neurons in the spinal cord for different sensory modalities, the distinct organization of their supraspinal neural networks has not been systematically explored. In the present study, we used HSV to efficiently achieve the polysynaptic infection of neural networks derived from Gal^+ nociceptors or Nts^+ pruriceptors. Gal^+ DRG neurons contain high level of tachykinin 1 ($Tac1$), $Calca$, and TRP cation channel, subfamily V, member 1 ($Trpv1$) (3, 4, 8), which can be activated by noxious heat. One subset of Gal^+ DRG neurons express $Trpm8$ at high level, which can be activated by innocuous to noxious cold temperatures (44, 45). Thus, it would be interesting to further investigate the network derived from the different subsets of Gal^+ DRG neurons in the future.

In the ascending pathway at the supraspinal level, the neural networks for pain and itch shared the spinobulbar projection but not the STT. It is well known that the VPL in the STT plays an essential role in the ascending pathway for processing the nociceptive information. Although participation of the VPL in processing itch has been reported in primates, its role in processing itch in rodents is vague. Identification of VPL in the neural network derived from Gal^+ nociceptors but not Nts^+ pruriceptors provides a clue for us to speculate the possible organization of ascending pathways for itch. For one possibility, other thalamic nuclei except the VPL may participate in processing itch from spinal cord to the SSp; another possibility is that itch might be encoded by neural networks derived from more than one type of pruriceptor. There are at least three types of pruriceptors, including the Nts^+, the $Mrgpra3^+$, and the $Mrgprd^+$ DRG neurons (3, 7). Generally, the Nts^+ and $Mrgpra3^+$ DRG neurons are pruriceptors for chemical itch, while the $Mrgprd^+$ DRG neurons are for mechanical itch (2). Therefore, the neural networks derived from different types of pruriceptors might encode different components of itch.

The spinobulbar projection connects to the limbic system (1), implying the participation of emotional aspects induced by pain and itch. The present study showed that the emotional motor system was involved in both networks but in different pathways. Neurons of the LPAG in the emotional motor system were labeled in the Gal^+ nociceptor network but not in the Nts^+ pruriceptor network. This subnucleus is known to control the defense and escape behaviors associated with pain sensation and threat (46). On the other hand, the NST and DMX in the emotional motor system mainly participated in the Nts^+ pruriceptor-derived neural network. The NST is a pair of nuclei known as the station for visceral sensation (47), and involved in the homeostatic system (48, 49). The close connection of NST/DMX with the limbic system suggests more emotional effects induced by itch. The DMX is located ventral to the NST, and performs the parasympathetic vagal functions in the cardiac, pulmonary, celiac, hepatic, mesenteric, and gastrointestinal tract via thoracic and abdominal vagal innervation (50). It would be of interest to further investigate the mechanisms of NST/DMX for arousing the compulsive desire for scratching.

RN is one of the most essential nuclei in the somatic motor system coordinating motor movements of the extremities (51). The role of the RN in the development of neuropathic pain has been intensively investigated (52). Previous studies on the RN indicated its participation in nociception and pathological pain. The fMRI studies revealed that the RN could be activated in response to painful stimuli (53). The functional connectivity of the RN was altered in migraine patients (54). Extracellular recording of magnocellular RN of the cat reveals that noxious heat activates those neurons (55). Moreover, the cytokines in the RN were involved in development and maintenance of neuropathic pain (56–58). We found that the labeling percentage of neurons in the MOp and RN derived from Gal^+ nociceptors was higher than that derived from Nts^+ pruriceptors, suggesting a more involvement of the somatic motor system in the pain-related network. This organization of neural network may underlie the mechanism of evasive action induced by noxious stimulations.

Functional Specificity of Networks Derived from Nociceptors and Pruriceptors. In order to validate the functional specificity of these two networks derived from Gal^+ nociceptors and Nts^+ pruriceptors, we examined the responsiveness of the PAG, RN, and NST/DMX to noxious heat or pruritic stimuli by detecting the c-Fos expression. Immediate early genes—such as Fos, $Egr1$, $Fosb$, and $Npas4$—are the most well-studied connection between the gene expression and the electrical and synaptic activity of neurons (59). The classically known activity-dependent transcription factors, including c-Fos, could be expressed immediately following stimulation in both excitatory and inhibitory neurons (60). Therefore, we use c-Fos to validate the functional specificity of the two networks in response to noxious or pruritic stimuli.

Generally, the nuclei expressing c-Fos induced by distinct modalities of stimuli were in accordance with that of the HSV labeling derived from specific types of DRG neurons. The extra nuclei with c-Fos expression compared with the tracing atlas imply that the labeling of the neural networks was incomplete, because the propagation time of the HSV tracer was limited. Moreover, pain and itch are multidimensional perceptions encompassing many physical and psychological components, and the nuclei in the anatomic network serve as the structural basis for processing the different components of sensory inputs. Therefore, a specific stimulus may not integrally activate all nuclei in the network. Importantly, the functional validation with chemogenetics revealed the role of RN in modulating pain-related evasive behavior and the NST/DMX in regulating

itch-aroused scratching. Our data show that the silencing of NST/DMX impaired the histamine-induced scratching behavior, but had no impact on cardiovascular activities at the resting state. One possible reason could be that the AAV used to deliver hM4Di employs a general *Ef1α* promoter, which would result in the expression of chemogenetic receptors in all infected cells. The NST/DMX may have both excitatory and inhibitory regulation of cardiovascular activities. The lack of cell-type selectivity for the silencing in the NST/DMX might underlie the failure in regulating cardiovascular activities. Furthermore, since the NST/DMX may participate in the transmission of visceral pain and drives autonomic responses, further studies are needed to determine if actual skin burn injury and tonic pain would activate the NTS/DMX, and if the NTS/DMX silencing would affect the tonic pain-associated behaviors.

In addition, we observed that silencing of the RN put a relatively modest impact on response to noxious heat in comparison with the dramatic increase caused by ablation of TRPV1$^+$ DRG neurons. The reason might be that TRPV1 is expressed in *Gal*$^+$, *Nts*$^+$, and *Mrgpra3*$^+$ DRG neurons. Thus, ablation of TRPV1-expressing neurons (61) affects not only *Gal*$^+$ DRG neurons but also other types of DRG neurons, as well as their downstream neural networks. Furthermore, silencing of the RN increased the exploratory locomotor activity of mice. Previous studies reported that some neurons in the RN participated in an inhibitory pathway for the breathing (62) and for the jaw-opening reflex (63). Prospectively, the neuron types in both common and differentially labeled nuclei could be identified by combining the viral tracing with single-cell RNA sequencing. The cellular and circuit mechanisms of the RN, NST/DMX, as well as other differentially labeled nuclei in regulation of pain and itch could be studied in the future.

Our database of mapping neural networks derived from *Gal*$^+$ nociceptors and *Nts*$^+$ pruriceptors systematically depict the subcortical nuclei in processing pain and itch, respectively. The anatomic differences of these two neural networks are dissected at the mesoscopic level. Candidate nuclei could be selected from this database for further functional study. Furthermore, we propose a way to isolate the neural network from a specific type of DRG neurons, and provide a strategy to investigate the neural mechanism for discrimination of different sensations. Based on the viral strategy, a functionally specific neural network could be also labeled with a recombinase to achieve the precise manipulation of neural circuit with the selective sensory modality.

Materials and Methods

All experiments presented in this study were conducted according to the guidelines of the Committee for Research and Ethical Issues of the International Association for the Study of Pain, and were approved by the Committee of Use of Laboratory Animals and Common Facility, the Center for Excellence in Brain Science and Intelligence Technology, Chinese Academy of Sciences, and the Guangdong Institute of Intelligence Science and Technology. Transgenic mice, viruses, antibodies, drugs, and experimental procedures are described in *SI Appendix, Materials and Methods*.

Data Availability. All study data are included in the main text and *SI Appendix*. Python scripts written by ourselves for determination of cell number in each nucleus are available in https://github.com/chenyan-sh/neuronCounting (64).

Author affiliations: ªGuangdong Institute of Intelligence Science and Technology, 519031 Zhuhai, China; ᵇInstitute of Neuroscience and State Key Laboratory of Neuroscience, Center for Excellence in Brain Science and Intelligence Technology, University of Chinese Academy of Sciences, CAS; Shanghai Research Center for Brain Science and Brain-Inspired Intelligence, Shanghai, 200031 China; ᶜResearch Unit of Pain Medicine, Chinese Academy of Medical Sciences; SIMR Joint Lab of Drug Innovation, Shanghai Advanced Research Institute, Chinese Academy of Sciences, Shanghai, 201210 China; ᵈNMPA Key Laboratory for Research and Evaluation of Viral Vector Technology in Cell and Gene Therapy Medicinal Products, Shenzhen Key Laboratory of Viral Vectors for Biomedicine, Brain Cognition and Brain Disease Institute, Shenzhen Institute of Advanced Technology, Chinese Academy of Sciences; Shenzhen-Hong Kong Institute of Brain Science-Shenzhen Fundamental Research Institutions, Shenzhen, 518055 China; ᵉSchool of Life Science and Technology, ShanghaiTec University, 201210 Shanghai, China; ᶠState Key Laboratory of Cell Biology, Shanghai Institute of Biochemistry and Cell Biology, Center for Excellence in Molecular Cell Science, Chinese Academy of Sciences, Shanghai, 200031 China; ᵍHuazhong University of Science and Technology-Suzhou Institute for Brainsmatics, Jiangsu Industrial Technology Research Institute for Brainsmatics, 215000 Suzhou, China; and ʰDepartment of Pain Medicine and Shenzhen Municipal Key Laboratory for Pain Medicine, Huazhong University of Science and Technology Union Shenzhen Hospital, Shenzhen, 518060 China

1. M. Ringkamp, S. N. Raja, J. N. Campbell, R. A. Meyer, "Peripheral mechanisms of cutaneous nociception" in *Wall & Melzack's Textbook of Pain*, S. B. McMahon, M. Koltzenburg, I. Tracey, D. C. Turk, Eds. (Elsevier Saunders, ed. 6, 2013), chap. 1, pp. 1–30.
2. M. Lay, X. Dong, Neural mechanisms of itch. *Annu. Rev. Neurosci.* **43**, 187–205 (2020).
3. C. L. Li et al., Somatosensory neuron types identified by high-coverage single-cell RNA-sequencing and functional heterogeneity. *Cell Res.* **26**, 83–102 (2016).
4. N. Sharma et al., The emergence of transcriptional identity in somatosensory neurons. *Nature* **577**, 392–398 (2020).
5. L. J. von Buchholtz et al., Decoding cellular mechanisms for mechanosensory discrimination. *Neuron* **109**, 285–298.e5 (2021).
6. K. Wang et al., Single-cell transcriptomic analysis of somatosensory neurons uncovers temporal development of neuropathic pain. *Cell Res.* **31**, 904–918 (2021).
7. D. Usoskin et al., Unbiased classification of sensory neuron types by large-scale single-cell RNA sequencing. *Nat. Neurosci.* **18**, 145–153 (2015).
8. A. Zeisel et al., Molecular architecture of the mouse nervous system. *Cell* **174**, 999–1014.e22 (2018).
9. L. Han et al., A subpopulation of nociceptors specifically linked to itch. *Nat. Neurosci.* **16**, 174–182 (2013).
10. K. K. Stantcheva et al., A subpopulation of itch-sensing neurons marked by Ret and somatostatin expression. *EMBO Rep.* **17**, 585–600 (2016).
11. Q. Liu et al., Mechanisms of itch evoked by β-alanine. *J. Neurosci.* **32**, 14532–14537 (2012).
12. J. Braz, C. Solorzano, X. Wang, A. I. Basbaum, Transmitting pain and itch messages: A contemporary view of the spinal cord circuits that generate gate control. *Neuron* **82**, 522–536 (2014).
13. J. Huang et al., Author correction: Circuit dissection of the role of somatostatin in itch and pain. *Nat. Neurosci.* **21**, 894 (2018).

14. L. Q. Luo, "Somatosensation: How do we sense body movement, touch, temperature, and pain?" in *Principles of Neurobiology* (Garland Science, 2015), pp. 269–272.
15. L. Q. Luo, "How is movement controlled?" in *Principles of Neurobiology* (Garland Science, 2015), pp. 326–350.
16. K. T. Beier et al., Anterograde or retrograde transsynaptic labeling of CNS neurons with vesicular stomatitis virus vectors. *Proc. Natl. Acad. Sci. U.S.A.* **108**, 15414–15419 (2011).
17. A. N. van den Pol, K. P. Dalton, J. K. Rose, Relative neurotropism of a recombinant rhabdovirus expressing a green fluorescent envelope glycoprotein. *J. Virol.* **76**, 1309–1327 (2002).
18. B. Zingg et al., AAV-mediated anterograde transsynaptic tagging: Mapping corticocollicular input-defined neural pathways for defense behaviors. *Neuron* **93**, 33–47 (2017).
19. D. Li et al., Anterograde Neuronal Circuit Tracers Derived from Herpes Simplex Virus 1: Development, Application, and Perspectives. *IJMS.* **21**, 5937 (2020).
20. X. Dong et al., Anterograde viral tracer hsv-1 strain h129 transports primarily as capsids in cortical neuron axons. *J. Virol.* **94**, e01957-19 (2020).
21. M. C. Zemanick, P. L. Strick, R. D. Dix, Direction of transneuronal transport of herpes simplex virus 1 in the primate motor system is strain-dependent. *Proc. Natl. Acad. Sci. U.S.A.* **88**, 8048–8051 (1991).
22. L. Lo, D. J. Anderson, A cre-dependent, anterograde transsynaptic viral tracer for mapping output pathways of genetically marked neurons. *Neuron* **72**, 938–950 (2011).
23. R. J. Whitley, B. Roizman, Herpes simplex virus infections. *Lancet* **357**, 1513–1518 (2001).
24. M. V. Mateos, J. F. San Miguel, Bortezomib in multiple myeloma. *Best Pract. Res. Clin. Haematol.* **20**, 701–715 (2007).
25. S. M. Schneider, B. H. Lee, A. V. Nicola, Viral entry and the ubiquitin-proteasome system. *Cell. Microbiol.* **23**, e13276–e13287 (2021).
26. A. M. Mitchell, R. J. Samulski, Mechanistic insights into the enhancement of adeno-associated virus transduction by proteasome inhibitors. *J. Virol.* **87**, 13035–13041 (2013).

27. A. E. McGovern et al., Distinct brainstem and forebrain circuits receiving tracheal sensory neuron inputs revealed using a novel conditional anterograde transsynaptic viral tracing system. *J. Neurosci.* **35**, 7041–7055 (2015).

28. Q. Wang et al., The Allen Mouse Brain Common Coordinate Framework: A 3D Reference Atlas. *Cell* **181**, 936–953.e20 (2020).

29. L. W. Swanson, Anatomy of the soul as reflected in the cerebral hemispheres: Neural circuits underlying voluntary control of basic motivated behaviors. *J. Comp. Neurol.* **493**, 122–131 (2005).

30. S. Davidson et al., Pruriceptive spinothalamic tract neurons: Physiological properties and projection targets in the primate. *J. Neurophysiol.* **108**, 1711–1723 (2012).

31. H. Mönnikes et al., Differential induction of c-fos expression in brain nuclei by noxious and non-noxious colonic distension: Role of afferent C-fibers and 5-HT3 receptors. *Brain Res.* **966**, 253–264 (2003).

32. Z. R. Gao et al., Tac1-expressing neurons in the periaqueductal gray facilitate the itch-scratching cycle via descending regulation. *Neuron* **101**, 45–59.e9 (2019).

33. V. E. Abraira, D. D. Ginty, The sensory neurons of touch. *Neuron* **79**, 618–639 (2013).

34. T. Liu, R. R. Ji, New insights into the mechanisms of itch: Are pain and itch controlled by distinct mechanisms? *Pflugers Arch.* **465**, 1671–1685 (2013).

35. P. T. Williams, J. H. Martin, Motor cortex activity organizes the developing rubrospinal system. *J. Neurosci.* **35**, 13363–13374 (2015).

36. E. T. Rolls, The cingulate cortex and limbic systems for emotion, action, and memory. *Brain Struct. Funct.* **224**, 3001–3018 (2019).

37. G. Paxinos, *The Rat Nervous System* (Academic Press, ed. 2, 1994), chap. 10, pp. 179–180.

38. M. Fujisaki, K. Hashimoto, M. Iyo, T. Chiba, Role of the amygdalo-hippocampal transition area in the fear expression: Evaluation by behavior and immediate early gene expression. *Neuroscience* **124**, 247–260 (2004).

39. S. Panteleev, D. Grundy, Descending influences from the infralimbic cortex on vago-vagal reflex control of gastric motor activity in the rat. *Auton. Neurosci.* **86**, 78–83 (2000).

40. B. L. Roth, DREADDs for neuroscientists. *Neuron* **89**, 683–694 (2016).

41. S. A. Connolly, J. O. Jackson, T. S. Jardetzky, R. Longnecker, Fusing structure and function: A structural view of the herpesvirus entry machinery. *Nat. Rev. Microbiol.* **9**, 369–381 (2011).

42. S. K. Mishra, M. A. Hoon, The cells and circuitry for itch responses in mice. *Science* **340**, 968–971 (2013).

43. Y. G. Sun et al., Cellular basis of itch sensation. *Science* **325**, 1531–1534 (2009).

44. D. A. Yarmolinsky et al., Coding and plasticity in the mammalian thermosensory system. *Neuron* **92**, 1079–1092 (2016).

45. M. Iftinca, C. Altier, The cool things to know about TRPM8! *Channels (Austin)* **14**, 413–420 (2020).

46. M. C. Chiang et al., Divergent neural pathways emanating from the lateral parabrachial nucleus mediate distinct components of the pain response. *Neuron* **106**, 927–939.e5 (2020).

47. C. B. Saper, The central autonomic nervous system: Conscious visceral perception and autonomic pattern generation. *Annu. Rev. Neurosci.* **25**, 433–469 (2002).

48. Y. M. Ulrich-Lai, J. P. Herman, Neural regulation of endocrine and autonomic stress responses. *Nat. Rev. Neurosci.* **10**, 397–409 (2009).

49. J. A. Ricardo, E. T. Koh, Anatomical evidence of direct projections from the nucleus of the solitary tract to the hypothalamus, amygdala, and other forebrain structures in the rat. *Brain Res.* **153**, 1–26 (1978).

50. H. Yuan, S. D. Silberstein, Vagus nerve and vagus nerve stimulation, a comprehensive review: Part I. *Headache* **56**, 71–78 (2016).

51. O. Devinsky, M. J. Morrell, B. A. Vogt, Contributions of anterior cingulate cortex to behaviour. *Brain* **118**, 279–306 (1995).

52. P. Boadas-Vaello, J. Homs, F. Reina, A. Carrera, E. Verdú, Neuroplasticity of supraspinal structures associated with pathological pain. *Anat. Rec. (Hoboken)* **300**, 1481–1501 (2017).

53. U. Bingel et al., Subcortical structures involved in pain processing: Evidence from single-trial fMRI. *Pain* **99**, 313–321 (2002).

54. X. Huang et al., Altered functional connectivity of the red nucleus and substantia nigra in migraine without aura. *J. Headache Pain* **20**, 104 (2019).

55. H. Steffens, J. A. Rathelot, Y. Padel, Effects of noxious skin heating on spontaneous cell activity in the magnocellular red nucleus of the cat. *Exp. Brain Res.* **131**, 215–224 (2000).

56. H. N. Li et al., Red nucleus IL-33 facilitates the early development of mononeuropathic pain in male rats by inducing TNF-α through activating ERK, p38 MAPK, and JAK2/STAT3. *J. Neuroinflammation* **18**, 150 (2021).

57. Q. Q. Yang et al., Red nucleus IL-6 mediates the maintenance of neuropathic pain by inducing the productions of TNF-α and IL-1β through the JAK2/STAT3 and ERK signaling pathways. *Neuropathology* **40**, 347–357 (2020).

58. Y. Y. Ding, H. N. Li, C. P. Ding, S. P. Han, J. Y. Wang, Red nucleus interleukin-1β evokes tactile allodynia through activation of JAK/STAT3 and JNK signaling pathways. *J. Neurosci. Res.* **96**, 1847–1861 (2018).

59. E. L. Yap, M. E. Greenberg, Activity-regulated transcription: bridging the gap between neural activity and behavior. *Neuron* **100**, 330–348 (2018).

60. I. Spiegel et al., Npas4 regulates excitatory-inhibitory balance within neural circuits through cell-type-specific gene programs. *Cell* **157**, 1216–1229 (2014).

61. S. K. Mishra, S. M. Tisel, P. Orestes, S. K. Bhangoo, M. A. Hoon, TRPV1-lineage neurons are required for thermal sensation. *EMBO J.* **30**, 582–593 (2011).

62. G. L. Ackland, R. Noble, M. A. Hanson, Red nucleus inhibits breathing during hypoxia in neonates. *Respir. Physiol.* **110**, 251–260 (1997).

63. Y. Chen et al., Distinct neural networks derived from galanin-containing nociceptors and neurotensin-expressing pruriceptors. GitHub. https://github.com/chenyan-sh/neuronCounting. Deposited 27 July 2022.

64. Y. Satoh, K. Ishizuka, S. Iwasaki, Role of the red nucleus in suppressing the jaw-opening reflex following stimulation of the raphe magnus nucleus. *Neurosci. Res.* **85**, 12–19 (2014).